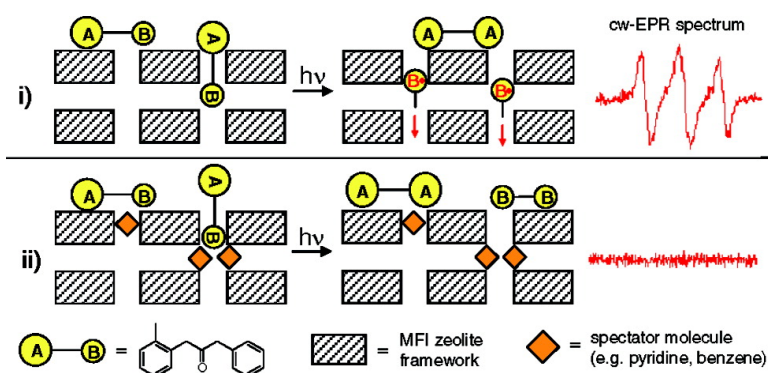Article

Photolysis of Dibenzyl Ketones Sorbed on MFI Zeolites in the Presence of Spectator Molecules: Cage Effects, Kinetics, and External Surface Sites Characterization

Alberto Moscatelli, Zhiqiang Liu, Xuegong Lei, Joanne Dyer,
Lloyd Abrams, M. Francesca Ottaviani, and Nicholas J. Turro

More About This Article

Additional resources and features associated with this article are available within the HTML version:

- Supporting Information
- Access to high resolution figures
- Links to articles and content related to this article
- Copyright permission to reproduce figures and/or text from this article

View the Full Text HTML

Photolysis of Dibenzyl Ketones Sorbed on MFI Zeolites in the Presence of Spectator Molecules: Cage Effects, Kinetics, and External Surface Sites Characterization[#]

Alberto Moscatelli,[§] Zhiqiang Liu,[§,†] Xuegong Lei,[§] Joanne Dyer,[§,‡] Lloyd Abrams,[‖] M. Francesca Ottaviani,[⊥] and Nicholas J. Turro*,[§]

Department of Chemistry, Columbia University, New York, New York 10027, Central Research and Development Department, DuPont Company, Wilmington, Delaware 19880, and Istituto di Scienze Chimiche, Università di Urbino, 61029 Urbino (PU), Italy

Received February 27, 2008; E-mail: njt3@columbia.edu

Abstract: Over the past two decades, the photolytic reactions of dibenzyl ketones sorbed on zeolites have been investigated. The reported results are consistent with a supramolecular model that takes into account the physical and chemical nature of the structure of the zeolites and their effect on the reactive radical intermediates produced by photolysis of adsorbed molecules. The model incorporates various phenomena such as surface coverage, external and internal sorption, surface diffusion, radical sieving, and the resulting product distributions. This account reports direct evidence for the validation of the model through FT-IR spectroscopy and through a new method for "titrating" the binding sites via EPR spectroscopy. It is shown that it is possible to adjust and modulate the photolytic product distribution by varying the parameters of the system. The effects of co-adsorbed spectator molecules with different polarities, namely water, pyridine, and benzene, on the photolysis of *o*-methyldibenzyl ketone and dibenzyl ketone sorbed on MFI zeolites is examined. This study provides insights into a displacement mechanism caused by spectator molecules and further demonstrates how the product distribution of photolysis of sorbed ketones can be controlled. The kinetics of persistent radicals formed by photolysis of ketones sorbed on zeolites is directly monitored over time by EPR, providing a measure of the lifetime of these reactive organic intermediates. Finally, measurement of Langmuir isotherms was employed to provide classical evidence for the model.

Introduction

Besides the variety of applications in industry and agriculture that have benefited from the use of zeolites,[1–4] these alumino-silicate crystals have also attracted the interest of chemists for basic science applications.[5–8] In particular, their channel systems and cavities have been useful as nanoreactors for chemical reactions.[9] External molecules sorb on the zeolite framework, forming intermolecular complexes that are addressed by the field of supramolecular chemistry. Even if not directly responsible for the bond-making and bond-breaking process, the chemistry of a reaction can be controlled by modulating the parameters of such intermolecular interactions. Normally, in the case of radical reactions in solution, statistics of radical–radical combination dominate the product distribution. However, using zeolites, the outcome of a radical–radical reaction can be controlled by supramolecular factors such as the binding strength and the location of the sorbed radical, as well as its available diffusion options. Through an understanding of the supramolecular structure and dynamics of the radical@zeolite[10] system, it is possible to control the product distribution of radical reactions and to diversify the photochemistry of isomeric precursors that would otherwise exhibit the same photochemistry in the solution phase.[11,12]

Figure 1 shows the size/shape dimensions of a series of dibenzyl ketones (DBKs) used as guest molecules (Chart 1) and the MFI zeolite-type framework used as the host system.[13] The cross section of *o*-MeDBK and *o,o'*-diMeDBK is ∼6.6 Å,

[#] Contribution no. 8853 from DuPont Co.

[§] Columbia University.

[‖] DuPont Company.

[⊥] Università di Urbino.

[†] Present address: Colgate-Palmolive Co., Piscataway, NJ 08855.

[‡] Present address: Art Conservation Research Center, Carnegie-Mellon University, Pittsburgh, PA 15219.

(1) Csicsery, S. M. *Pure Appl. Chem.* **1986**, *58*, 841.

(2) Mumpton, F. A. *Proc. Natl. Acad. Sci. U.S.A.* **1999**, *96*, 3463.

(3) Newsam, J. M. *Science* **1986**, *231*, 1093.

(4) Breck, D. W. *Zeolite Molecular Sieves: Structure, Chemistry, and Use*; Krieger Publishing Co.: Melbourne, FL, 1984.

(5) Calzaferri, G.; Huber, S.; Maas, H.; Minkowski, C. *Angew. Chem., Int. Ed.* **2003**, *42*, 3732.

(6) Sivaguru, J.; Shailaja, J.; Ramamurthy, V. In *Handbook of Zeolite Science and Technology*; Auerbach, S. M., Carrado, K. A.;, Dutta, P. K., Eds.; Marcel Dekker: New York, 2003.

(7) Tung, C.-H.; Wu, L.-Z.; Zhang, L.-P.; Chen, B. *Acc. Chem. Res.* **2003**, *36*, 39.

(8) Chretien, M. N. *Pure Appl. Chem.* **2007**, *79*, 1.

(9) Tretyakov, Y. D.; Lukashin, A. V.; Eliseev, A. A. *Russ. Chem. Rev.* **2004**, *73*, 899.

(10) The nomenclature probe@zeolite is adopted to represent the supramolecular complex of a guest probe molecule sorbed on zeolite in analogy to the common guest@host representation of supramolecular systems.

(11) Turro, N. J.; Cheng, C. C.; Lei, X. G.; Flanigen, E. M. *J. Am. Chem. Soc.* **1985**, *107*, 3739.

(12) Garciagaribay, M. A.; Zhang, Z. Y.; Turro, N. J. *J. Am. Chem. Soc.* **1991**, *113*, 6212.

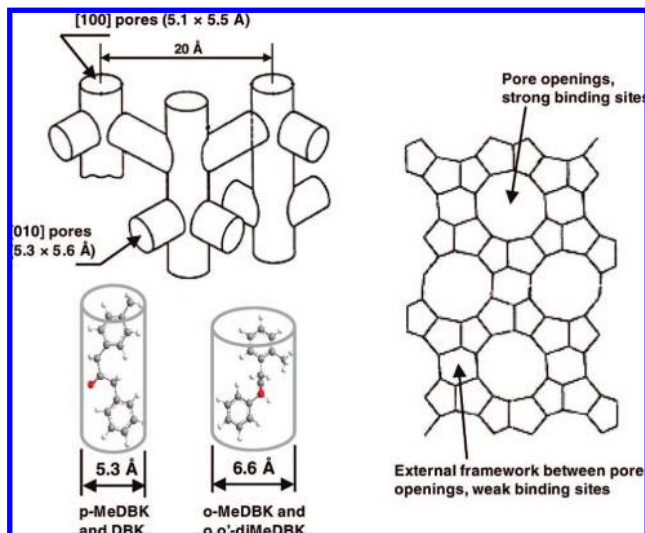(13) Baerlocher, C.; Meier, W. M.; Olson, D. H. *Atlas of Zeolite Framework Types*; Elsevier: Amsterdam, 2001.

Figure 1. MFI zeolite framework and kinetic diameter of *p*-MeDBK (and DBK) and *o*-MeDBK (and *o,o′*-diMeDBK). Pore-opening sizes are also reported, according to ref 13. The external surface is composed of strong binding sites located at the pore openings and weak binding sites located in the external framework of the zeolite between the pores.

Chart 1. Dibenzyl Ketones Investigated in the Present Work
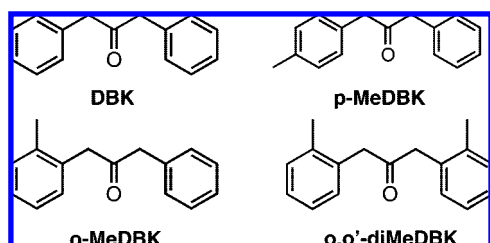
whereas for DBK and *p*-MeDBK it is ~5.3 Å.[14] Since the diameter of the pore opening for MFI zeolites is ~5.5 Å, DBK and *p*-MeDBK can be absorbed inside the zeolite pore openings and diffuse into the internal surface. By contrast, *o*-MeDBK can be adsorbed in the pore opening but cannot diffuse into the internal surface because of the ortho-methyl substitution. Finally, *o,o′*-diMeDBK cannot absorb in the pore openings and therefore must be entirely adsorbed on the external surface.

The paradigm or model employed to rationalize the results of photolysis of these ketones, along with the scientific facts that led to its development and support it, is described in detail in a recent review.[15] The model takes into account the sieving ability of the zeolites and considers the size/shape/diffusion characteristics of the photolytic fragments in terms of two different initial surface-binding sites of the external surface (Figure 1): strong binding sites, located at the pore openings, at which adsorbed molecules interact by hydrogen-bonding and/ or partial intercalation, and weak binding sites, located at the surface "non-openings" of the zeolite framework, at which hydrogen-bonding and/or van der Waals interactions take place. Strong binding sites are occupied first, whereas weak binding sites are occupied when the former become saturated.[16] Solid-state NMR and EPR spectroscopies have provided direct

(14) Li, W. Ph.D. Dissertation, Columbia University, New York, NY, 1999.
(15) Turro, N. J. *Acc. Chem. Res.* **2000**, *33*, 637.
(16) Hirano, T.; Li, W.; Abrams, L.; Krusic, P. J.; Ottaviani, M. F.; Turro, N. J. *J. Org. Chem.* **2000**, *65*, 1319.
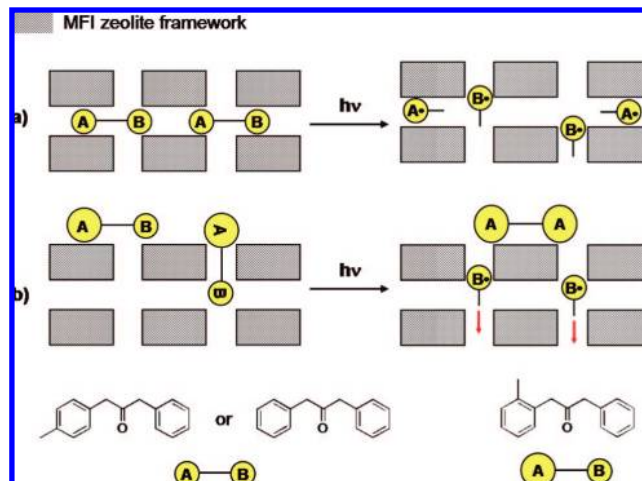
Figure 2. Schematic representation of photolysis of DBKs@MFI zeolite. (a) *p*-MeDBK or DBK is absorbed inside the zeolite channel system and, upon photolysis, they form persistent A• and B• benzyl radicals. As discussed in the text, the product distribution, measured by cage effect, changes dramatically upon adding spectator molecules that displace *p*-MeDBK or DBK toward the external surface. (b) *o*-MeDBK can only adsorb on the external surface, either by van der Waals interactions, hydrogen-bonding, or intercalation inside the pores with the unsubstituted benzene ring. Photolysis of *o*-MeDBK@MFI produces persistent benzyl radical B• that sieves inside the pore system and transient radical A• that readily combines to form A–A product.

evidence for the sites of adsorbed molecules.[17] It was possible, for instance, to characterize quantitatively the strong binding sites[18–20] as well as to elucidate the high mobility of adsorbate molecules on the zeolite surface.[20–22] In this paper, these studies are extended to provide direct evidence for validation of the model for the external surface of zeolite by FT-IR spectroscopy. In addition, a new method for "titrating" the strong binding sites by EPR spectroscopy is developed. The binding energies between selected adsorbate molecules and the external surface of zeolites are evaluated by the Langmuir isotherm method.

The adsorption sites of the initially adsorbed ketones and the radicals produced by photolysis are shown schematically in Figure 2. The geminate radical pair (A• + B•) is produced by photodecomposition followed by rapid decarbonylation (Scheme 1). There are several possibilities for product formation, depending on the initial location of the ketone on the zeolite (Figure 2). According to the model, three possible cases are assumed: (i) the ketone is entirely inside the internal surface of the zeolite (absorption); (ii) the ketone is interacting entirely on the external surface of the zeolite (adsorption); and (iii) the ketone is partially on the external surface and partially in the pores leading to the internal surface (sorption). For case (i), the geminate radical pair (A• + B•) is not expected to be able to diffuse apart readily because both partners are constrained by

(17) Turro, N. J.; Lei, X. G.; Li, W.; Liu, Z. Q.; Ottaviani, M. F. *J. Am. Chem. Soc.* **2000**, *122*, 12571.
(18) Liu, Z. Q.; Ottaviani, M. F.; Abrams, L.; Lei, X. G.; Turro, N. J. *J. Phys. Chem. A* **2004**, *108*, 8040.
(19) Ottaviani, M. F.; Lei, X. G.; Liu, Z. Q.; Turro, N. J. *J. Phys. Chem. B* **2001**, *105*, 7954.
(20) Turro, N. J.; Lei, X. G.; Li, W.; Liu, Z. Q.; McDermott, A.; Ottaviani, M. F.; Abrams, L. *J. Am. Chem. Soc.* **2000**, *122*, 11649.
(21) Turro, N. J.; Lei, X. G.; Li, W.; McDermott, A.; Abrams, L.; Ottaviani, M. F.; Beard, H. S. *Chem. Commun.* **1998**, 695.
(22) Turro, N. J.; McDermott, A.; Lei, X. G.; Abrams, L.; Ottaviani, M. F.; Beard, H. S.; Houk, K. N.; Beno, B. R.; Lee, P. S.; Li, W. *Chem. Commun.* **1998**, 697.

Scheme 1. Reaction Scheme for the Photolysis of Dibenzyl Ketones and Recombination Cases in Supramolecular Systems
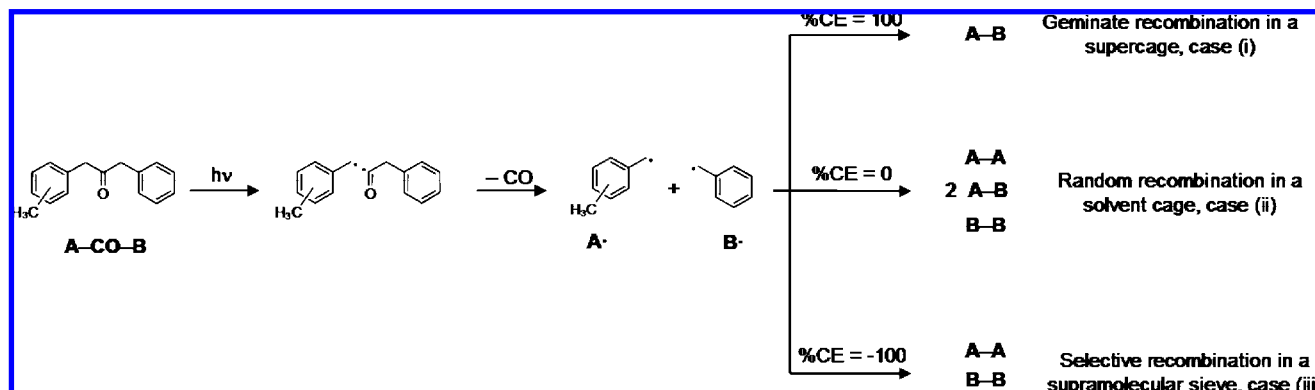
the walls of the host structure. Thus, the main product of the photolysis is the geminate coupling product A−B, corresponding to a limiting cage effect of +100%. For case (ii), the geminate radical pair (A$^{\bullet}$ + B$^{\bullet}$) may be able to diffuse rapidly apart, considering the expected weak binding of the radicals by the external surface. In this case, a statistical set of recombination products A−A, A−B, and B−B is expected in the limit of complete and irreversible diffusional separation of the geminate pair, corresponding to a limiting cage effect of 0%. For case (iii), the partners of the geminate radical pair (A$^{\bullet}$ + B$^{\bullet}$) are sorbed in two distinct locations of the zeolite structure: one partner is weakly bound to the external surface and is too large to diffuse into the pores of the internal surface, and the other partner is adsorbed in a pore strategically poised to be absorbed into the internal surface. In this case, in the limit where diffusion into the internal surface is fast and irreversible compared to geminate combination, the major products are expected to be A−A and B−B, corresponding to a limiting cage effect of −100%.

Equation 1 defines a "cage effect" (%CE) for the three cases above, based on measurement of the product distribution of A−A, A−B, and B−B. Thus, working backward from the product distribution, the initial site of the ketone probe can be computed from simple measurement of the eventual product distribution produced by the initially geminate radical pair (A$^{\bullet}$ + B$^{\bullet}$).

$$\%CE = \frac{AB - (AA + BB)}{AA + AB + BB} \tag{1}$$

It is possible to adjust and modulate the photolytic product distribution by changing various parameters of the system, such as Al content of zeolite, charge-compensating counterion, loading of adsorbed molecule, and amount of co-adsorbed spectator molecules. In this paper, the effect of co-adsorbed spectator molecules with different polarity, namely water, pyridine, and benzene, on the photolysis of DBKs@MFI is investigated. This study permits the elucidation of the displacement mechanism by spectator molecules and further demonstrates the ability to modify product distribution and the cage effect. In addition, the kinetics of persistent radicals formed by photolysis is followed over time by continuous wave EPR (cw-EPR) to measure their lifetimes.[23]

The importance of investigating the external surface of zeolites resides also in the fact that the first step for the interaction of any guest molecule with zeolites is the adsorption onto the external surface, followed by a size/shape-selective diffusion inside the internal pores.[24,25] The impact of this first step on the performance of zeolites depends on the particle size of the zeolite crystal, because the external surface area (S_{ext}) increases faster than the internal surface area as particle size decreases. Simple geometrical reasoning for a model of a cubic particle of side *l* yields eq 2,

$$\frac{S_{ext}}{S_{tot}} = \frac{1}{l} \tag{2}$$

where S_{tot} is the total surface area of the zeolite.

Results and Discussion

Photolysis of DBK@MFI: Cage Effect and Kinetics. At low loadings, water acting as a co-adsorbed "spectator" molecule displaces DBK from the hydrophilic, Al-containing sites located in the internal channels, as demonstrated by the decrease of the cage effect with increasing water molecule loading.[26] However, this is strictly true only for zeolites with high Al content (Si/Al < 20). The cage effect versus water loading plot displays a minimum for zeolites with higher Si−Al ratio.[27] This was rationalized by supposing that the displacement is effective up to a certain amount of water, corresponding to the saturation of the Al sites. Additional water probably forms globules within the zeolite channels, thereby restricting migration of radicals and fostering recombination (resulting in a high cage effect). However, ketones adsorbed on hydrophobic sites inside the channels system are not displaced by water. In fact, DBK remains trapped in the hydrophobic portions of the channels as the cage effect increases after reaching a minimum. Figure 3 shows plots of the cage effect versus water loading for MFI zeolite type with different Si−Al ratios. Only for very hydrophobic sites with high aluminum contents, such as Si/Al = 13, does the cage effect decrease monotonically with water loading. For Si/Al ratios >13, a minimum is found; its position shifts toward lower water loadings with decreasing Al content. Quantitatively, there exists a good correlation (Table 1) between the water content calculated assuming a 6:1 ratio of H_2O to Al and the percentage of water at the minimum of the cage effect curve of Figure 3; this explains the cage effect behavior in terms of the Al content of the zeolite.

(23) Turro, N. J.; Jockusch, S.; Lei, X. G. *J. Org. Chem.* **2002**, *67*, 5779.

(24) Gilson, J. P.; Derouane, E. G. *J. Catal.* **1984**, *88*, 538.
(25) Kennedy, C. R.; Lapierre, R. B.; Pereira, C. J.; Mikovsky, R. J. *Ind. Eng. Chem. Res.* **1991**, *30*, 12.
(26) Turro, N. J.; Wan, P. *J. Am. Chem. Soc.* **1985**, *107*, 678.
(27) Turro, N. J.; Cheng, C. C.; Abrams, L.; Corbin, D. R. *J. Am. Chem. Soc.* **1987**, *109*, 2449.
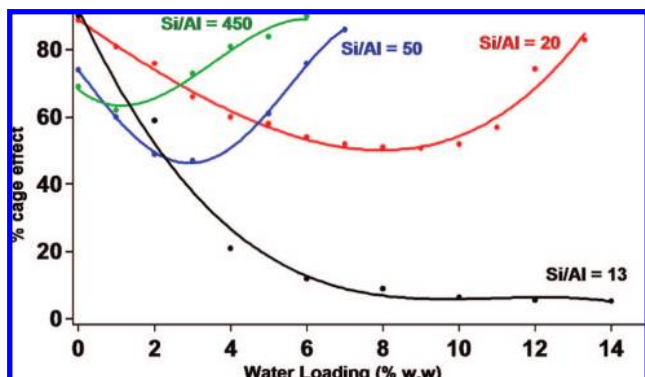
Figure 3. Plot of % cage effect versus % water loading for ZSM-5 zeolite with different Si-Al ratios. The polynomial fitting curve is only for visual purposes and has no physical meaning.

Table 1. Percentage of Water Absorbed in the MFI Zeolites, Evaluated by Cage Effect (CE) Measurements[a]

Si/Al	x	wt % H_2O (6:1)	CE minimum (wt % H_2O)
13	6.9	13	
20	4.5	8.3	8.5 ± 0.5
50	1.9	3.5	3 ± 0.5
450	0.21	0.40	1 ± 0.5

[a] Unit-cell formula: $Na_xSi_{(96-x)}Al_xO_{192}$.[13] The minima of Figure 3 agree quite well with the calculated value for a H_2O−Al ratio of 6:1.[27,56]
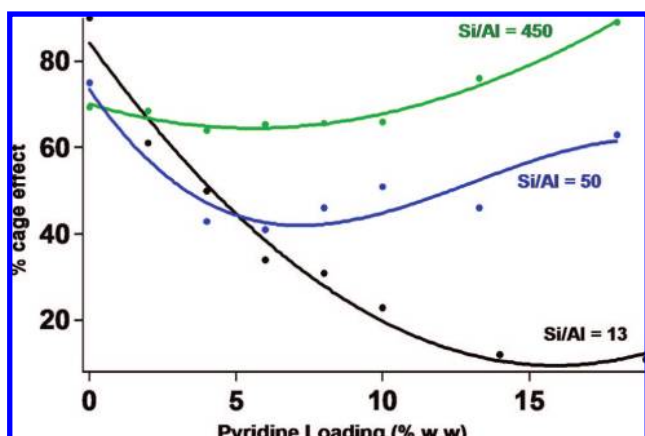

Figure 4. Plot of % cage effect versus % pyridine loading for ZSM-5 zeolite with different Si-Al ratios. The polynomial fitting curve is only for visual purposes and has no physical meaning.

The same qualitative results as found for water are also observed for pyridine as a spectator molecule (Figure 4). Pyridine exhibits strong binding to the Al-containing sites[28] that enables the displacement of DBK from the hydrophilic sites, thereby decreasing the cage effect. At high loadings, pyridine displaces DBK into the hydrophobic portion of the zeolite channels, inhibits radical diffusion, and raises the cage effect.

Hindered diffusion inside the zeolite channels causes the benzyl radical pair produced by the photodecomposition of DBK, followed by fast decarbonylation, to be persistent and detectable by cw-EPR spectroscopy at room temperature.[29,30] In Figure 5, the cw-EPR spectra upon photolysis of 1% loading

(28) Scaiano, J. C.; Kaila, M.; Corrent, S. *J. Phys. Chem. B* **1997**, *101*, 8564.

(29) Turro, N. J.; Lei, X. G.; Jockusch, S.; Li, W.; Liu, Z. Q.; Abrams, L.; Ottaviani, M. F. *J. Org. Chem.* **2002**, *67*, 2606.
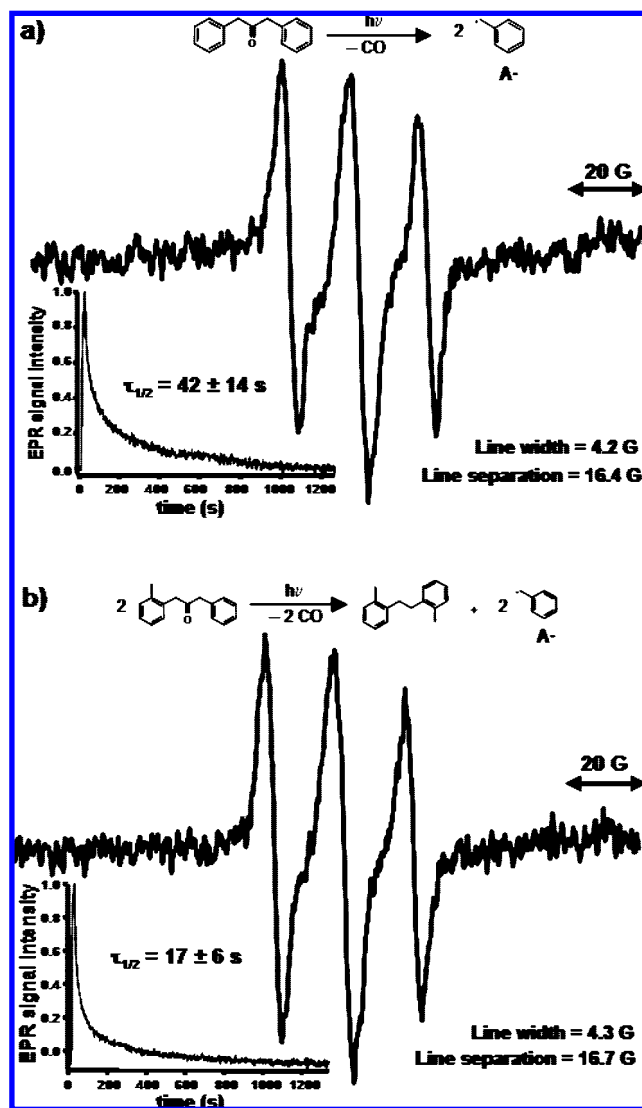
Figure 5. EPR spectra after photolysis of (a) 1% loading DBK@MFI (Si/Al = 20) and (b) 1% loading of *o*-MeDBK@MFI (Si/Al = 20) with the respective signal evolution over time. Line width and hyperfine coupling constant with the two methylene hydrogens (a_H) are also reported. Time evolution is recorded at the top of the central line, and its value is the result of three independent measurements.

of DBK@MFI (Si/Al = 20) and o-MeDBK@MFI (Si/Al = 20) are reported: both show a three-line spectrum as expected from hyperfine interaction of the unpaired electron with the two methylene hydrogens.[31] Under these conditions, the benzyl radical half-lifetime is 42 ± 14 s. As a benchmark, diffusion-controlled radical−radical reactions in nonviscous solvents results in radical lifetimes of the order of 10^{-6} s. Such short-lived radicals cannot be easily detected by cw-EPR and are termed "transient". Since the benzyl radicals that carry the signal of Figure 5 are many orders of magnitude longer lived, they are termed "persistent".

The presence of spectator molecules in the EPR spectra resulting upon photolysis of DBK@MFI was investigated (Figure 6). Addition of benzene or pyridine above 2% loading

(30) Pushkara Rao, V.; Zimmt, M. B.; Turro, N. J. *J. Photochem. Photobiol. A* **1991**, *60*, 355.

(31) For these measurements, deuterated benzene rings were employed in order to avoid complicated EPR spectra due to the hyperfine splitting with benzene protons.
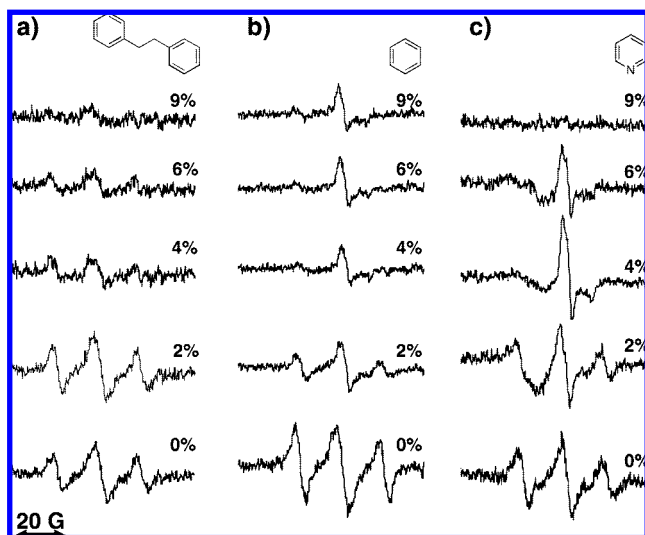
Figure 6. EPR spectrum after irradiation of 1% DBK@MFI (Si/Al = 20) in the presence of (a) diphenylethane, (b) benzene, and (c) pyridine at different loadings.

totally "quenches" the benzyl EPR signal (Figure 6b,c). This is explained by the model as follows: Before photolysis, as the system is in equilibrium, the added spectator molecules displace the initially sorbed DBK located in the internal channels to the external surface. Photolysis produces benzyl radicals on the external surface, where radical mobility is greater and recombination occurs rapidly. As a result, the benzyl radical that is "persistent" (long-lived) in the absence of benzene or pyridine become "transient" (short-lived) in the presence of these spectator molecules. This observation is in agreement with the decrease of the cage effect with increased loading of spectator molecules (Figures 3 and 4). Interestingly, at loadings greater than 2% a new persistent two-line EPR spectrum appears (Figure 6b,c). The shape of the spectrum is characteristic of an acetyl radical adsorbed on a surface.[32,33] Considering the photochemistry of the system, the signal is assigned to the phenylacetyl radical formed after Norrish type I photoreaction (α-cleavage) of DBK as primary photochemical product, or from the secondary photolysis of the rearrangement product methyldeoxybenzoin. A control experiment shows that the photolysis of 4-methylbenzyl phenyl ketone on ZSM-5 produces a superposition of EPR spectra of benzyl and benzoyl radicals, a feature not observed in our study. Therefore, it is concluded that the acetyl signal in Figure 6b,c derives from the phenylacetyl radical. Decarbonylation of phenylacetyl radicals in solution occurs in microseconds or less.[34,35] In general, also in the zeolite media, decarbonylation occurs too fast for the cw-EPR to be able to follow it.[36] However, in the case of the Figure 6b,c, decarbonylation of phenylacetyl radical, a unimolecular process, is inhibited and causes the radical to be persistent. The mechanism for the inhibition of decarbonylation by the high

concentration of spectator molecules is not obvious. It is proposed that, at high concentrations of spectator molecules, the latter can tightly pack within the zeolite channels and prevent diffusion of the CO from the immediate vicinity of the benzyl radical. An equilibrium is thus set up between the phenylacetyl radical and the benzyl radical and CO. In this way, the concentration of phenylacetyl radical at equilibrium is sufficient to allow its detection. By comparison, the spectator molecule diphenylethane (Figure 6a), which because of its large size packs more loosely within the zeolite channels, produces only a reduction of the benzyl radical lifetime with increasing loading, as a result of DBK displacement from the internal channels.

Photolysis of *o*-MeDBK@MFI: Kinetics. During the photodecomposition of *o*-MeDBK@MFI, the smaller benzyl radical B• is initially located at or near the pore opening at the external surface (since *o*-MeDBK is initially located at the strong binding sites at the pores). Since the kinetic diameter of B• is smaller that the size of the pore opening, it can sieve into the channel system and becomes persistent. On the other hand, the large *o*-methylbenzyl radical (A•) possesses a kinetic cross section larger than the pore openings and thus is unable to percolate into the channels. As a result, A• radicals diffuse readily on the external surface and recombine with other A• radicals, thus being transient (Figure 2). Consequently, only the persistent B• radicals that have sieved into the internal surface are seen in the cw-EPR spectra after the photolysis of *o*-MeDBK@MFI.[29] Figure 5b shows the time-dependent EPR spectrum after photolysis of 1% loading *o*-MeDBK@MFI (Si/Al = 20). The three-line spectrum validates the attribution to the benzyl radical. Moreover, *o*-methylbenzyl radical (A•) would be easily recognizable by EPR due to a different hyperfine pattern. For the spectra in Figure 5, the EPR parameters, such as the line width and the hyperfine coupling constant (a_H), are very similar. However, the slightly smaller value of a_H (a signature of a lower polarity environment)[37] for the spectrum in Figure 5a is consistent with a more hydrophobic environment sensed by the benzyl radical inside the internal channels, resulting from a difference in the initial location of the benzyl radical precursors, DBK and *o*-MeDBK.

Addition of 4% loading of pyridine or 6% loading of *p*-xylene "quenches" the EPR spectrum completely (Figure 7). This result is consistent with the spectator molecules readily absorbing into the channel system, displacing the adsorbed ketones to the external surface, and also inhibiting the sieving of the photolysis products from the external surface to the internal surface. As a result, the B• radicals produced by photolysis are restricted to the external surface, transforming B• radicals from persistent to transient.[38]

Titration of the Strong Binding Sites on the External Surface of MFI Zeolite by EPR Spectroscopy. There are two important reasons why nitroxides have been used to probe and characterize zeolite surfaces: (i) the high sensitivity of the EPR technique, which allows very low loadings of adsorbed probe

(32) Fischer, H. In *Magnetic Properties of Free Radicals*; Hellwege, K.-H.; Hellwege, A. M., Eds.; Landolt−Börnstein: Group II Molecules and Radicals; Springer-Verlag: Berlin, 1965.

(33) Turro, N. J.; Lei, X. G.; Niu, S. F.; Liu, Z. Q.; Jockusch, S.; Ottaviani, M. F. *Org. Lett.* **2000**, *2*, 3991.

(34) Lunazzi, L.; Ingold, K. U.; Scaiano, J. C. *J. Phys. Chem.* **1983**, *87*, 529.

(35) Turro, N. J.; Gould, I. R.; Baretz, B. H. *J. Phys. Chem.* **1983**, *87*, 531.

(36) Lei, X.; Jockusch, S.; Ottaviani, M. F.; Turro, N. J. *Photochem. Photobiol. Sci.* **2003**, *2*, 1095.

(37) Ottaviani, M. F.; Martini, G.; Nuti, L. *Magn. Reson. Chem.* **1987**, *25*, 897.

(38) Because the samples in Figures 6 and 7 are loaded with the same amount of ketone and irradiated for the same amount of time, and the spectra are acquired under the same physical and instrumental conditions, they also provide an integrated snapshot of the kinetic profile from 0 to 24 s from the end of the irradiation, where 24 s is the time taken to acquire the cw-EPR spectrum. Therefore, the fact that, at high loading of spectator molecule, the spectrum of benzyl radical disappears indicates a shorter lifetime under such conditions, in accordance with the model of Figure 2.
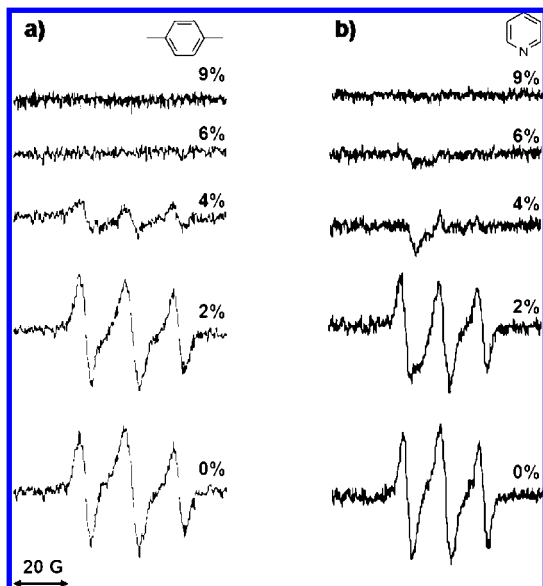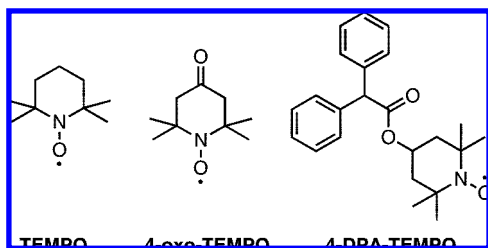
Figure 7. EPR spectrum after irradiation of 1% *o*-MeDBK@MFI (Si/Al = 20) in the presence of (a) *p*-xylene and (b) pyridine.

Chart 2. Structures of the Nitroxide Probes Used in the Present Work

(on the order of $10^{-3}\%$ by weight)[39] to be studied, and (ii) the ability to measure the mobility and the environmental polarity of the probes, because of the dramatic change of line shape of their EPR spectra under hindered conditions and the sensitivity of a_H to the polarity of the environment.[40] As a result, EPR provides a very elegant method to discriminate probes adsorbed on relatively strong binding sites from probes adsorbed on relatively weak binding sites. [20] In this paper, a direct method to "titrate" the strong binding sites and to distinguish them from the weak binding sites on the external surface of zeolites is developed. In order to restrict variables that might influence the pertinent parameters, monodisperse MFI silicalite crystals (synthesized as per the Experimental Section) are used. These crystals possess virtually no Al (Si/Al > 1000). Both 4-DPA-TEMPO and 4-oxo-TEMPO (Chart 2) are employed as EPR probes. These two probes were chosen because they have a low and a high interacting strength toward the surface sites, respectively.[18] Furthermore, the TEMPO moiety, with its kinetic diameter of 11 Å, adsorbs exclusively on the external surface of MFI zeolite crystals.[41]

(39) For such low loaded zeolites, in order to avoid exponential numbers in the percentage, it is usually preferable to use millimolality (m*m*, millimoles of adsorbate per gram of zeolite). However, in this paper, we choose to keep percentage for consistency and comparison

(40) *Spin Labeling: Theory and Applications*; Berliner, L. J., Ed.; Academic Press: New York, 1976.

(41) Khodakov, A. Y.; Kustov, L. M.; Bondarenko, T. N.; Dergachev, A. A.; Kazansky, V. B.; Minachev, K. M.; Borbely, G.; Beyer, H. K. *Zeolites* **1990**, *10*, 603.
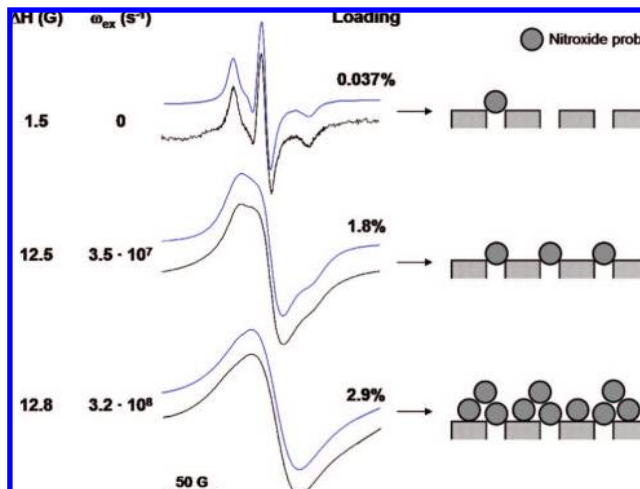
Figure 8. 4-DPA-TEMPO EPR spectra at different loadings (black line), with relative simulation (blue line), and schematic representation of the loading of the external surface of zeolite in the light of the model described in the text. The intrinsic line width (Δ*H*) and the spin−spin exchange frequency (ω_{ex}) used to obtain the simulated spectra are reported. They are averages of the all probes adsorbed onto the different binding sites. These spectra refer to the silicalite S_1.

In Figure 8, 4-DPA-TEMPO EPR spectra, at different surface loadings, are shown (simulated spectra shown on upper traces): line shapes are very dependent on the loading, and in particular, the three hyperfine lines broaden to complete coalescence around 1.8% loading. A schematic interpretation of the EPR spectra in terms of the location of the probes on the external surface is presented to the right of each spectrum. The line shapes of the spectra in Figure 8 for the 1.8% loading (and lower loadings) are consistent with the partial resolution of the magnetic dipole−dipole interaction anisotropies. This interaction depends on the distance and on the relative orientation of the magnetic dipoles and is modulated by the rotational diffusion motion of the probe. The probe is expected to first bind to the strong binding sites on the external surface. Because of this interaction, the probe's motion is inhibited. As a result, the dipole−dipole interaction between electron spins does not average to zero (as it does when there is fast isotropic motion of the probe). Under the assumption that the broadening is dominated by dipolar interactions between adjacent inhibited probes in strong binding sites, the following simple relationship between the average probe distance (*d*, expressed in Å) and spectral line width (ΔH_d, in G) has been developed:[42−44]

$$\Delta H_d = 3 \times 10^4 \left(\frac{1}{d^3}\right) \qquad (3)$$

Equation 3 provides a means of determining the distance between adjacent spin probes on the external surface of silicalite.

However, since the dipole−dipole interaction only accounts for the line broadening and does not explain the observed coalescence of the hyperfine lines, it is necessary to take into consideration the spin−spin exchange mechanism between probes adsorbed on the weak binding sites of the external surface of zeolite. This interaction occurs when the probes undergo free diffusion and collide at a certain frequency (as in the case of very concentrated solutions), thus undergoing overlapping

(42) Sackmann, E.; Trauble, H. *J. Am. Chem. Soc.* **1972**, *94*, 4482.
(43) Sackmann, E.; Trauble, H. *J. Am. Chem. Soc.* **1972**, *94*, 4492.
(44) Trauble, H.; Sackmann, E. *J. Am. Chem. Soc.* **1972**, *94*, 4499.

Table 2. Critical Loading Values (*c**) and Corresponding Average Probe Distance for Different MFI Zeolites

symbol[a]	Si/Al[b]	ESA[c] $(m^2 \cdot g^{-1})$	EPR probe	c^* (wt %) measd	c^* (wt %) calcd	distance at c^* (Å)
S_1	>1000	55.1	4-DPA-TEMPO	1.83	1.89	13.4
S_2	>1000	20.3	4-DPA-TEMPO	0.66	0.70	13.3
S_3	>1000	9.27	4-DPA-TEMPO	0.35	0.32	13.3
S_4	>1000	5.71	4-DPA-TEMPO	0.17	0.20	13.0
S_5	>1000	29.8	4-DPA-TEMPO	0.92	1.02	12.7
S_6	>1000	3.75	4-DPA-TEMPO	0.04	0.13	13.2
S_7	>1000	2.75	4-DPA-TEMPO	0.02	0.05	13.1
S_7	>1000	2.75	4-oxo-TEMPO	0.02	0.05	12.7
C_1	1000		4-oxo-TEMPO	0.017		13.2
C_2	400		4-oxo-TEMPO	0.013		13.0
C_3	90		4-oxo-TEMPO	0.051		12.9

[a] Home-made silicalites have symbol S_n, and commercial zeolites have symbol C_n. [b] Si/Al > 1000 corresponds to silicalite crystals. [c] Measured by mercury porosimetry.

orbitals. In order to distinguish the portion of line width that originates from the dipole−dipole mechanism and the spin exchange, a computer-aided simulation of the adsorbed nitroxide probes spectra is performed. The simulation procedure is described in the Experimental Section. Some representative simulation output spectra are shown in Figure 8 as the upper traces, along with the corresponding values of line broadening (ΔH) and spin exchange frequency (ω_{ex}).

From the simulations, at low surface coverage (0.037%), the EPR spectrum of 4-DPA-TEMPO displays a line shape that is characteristic of nitroxide probes undergoing slow rotational motion. Furthermore, the spectrum can be simulated without inclusion of any spin-exchange interaction and is only slightly broadened by the dipole−dipole interaction. For such a spectrum, $\Delta H = 1.5$ G, which converts to a probe distance of 27 Å using eq 3.

By tracking the EPR parameters as a function of loading, the spectra are found to exhibit a qualitative change in parameters at a loading of ~1.8%. This change is considered a signature of the saturation of the strong binding sites and the onset of the transition to occupation of the weak binding sites. This loading is termed a "critical" loading (c^*). At c^*, the computation indicates the maximum value for the line width, $\Delta H = 12.5$ G, which corresponds to a probe separation of 13.4 Å. At this distance, a small spin-exchange contribution is needed to properly simulate the spectrum ($\omega_{ex} = 3.5 \times 10^7$ s^{-1}). It is noteworthy that the distance between the centers of the pore openings on the silicalite external [010] surface is 12 Å and that on the [001] surface is 14 Å, as measured by XRD.[45] This excellent agreement between the probe separation from eq 3 and the pore separation distance measured by XRD is consistent with the saturation of the pore opening at c^*.

At a surface coverage of 2.9%, the EPR spectrum of the probe collapses to a single line. Simulation indicates an electron−electron exchange interaction ($\omega_{ex} = 3.2 \times 10^8$ s^{-1}), in addition to a strong but essentially constant dipolar broadening ($\Delta H = 12.8$ G ≡ 13.3 Å). These results are consistent with the hypothesis of a constant dipolar contribution when the pores are saturated and with a loading-dependent contribution from spin−spin interactions above c^*. To test this hypothesis, the EPR spectra for monodisperse zeolite crystal of different sizes (S_1 to S_7, Table 2) were measured as a function of loading, and the values of c^* were evaluated by simulation of the spectra. Although the

(45) Flanigen, E. M.; Bennett, J. M.; Grose, R. W.; Cohen, J. P.; Patton, R. L.; Kirchner, R. M.; Smith, J. V. *Nature* **1978**, *271*, 512.
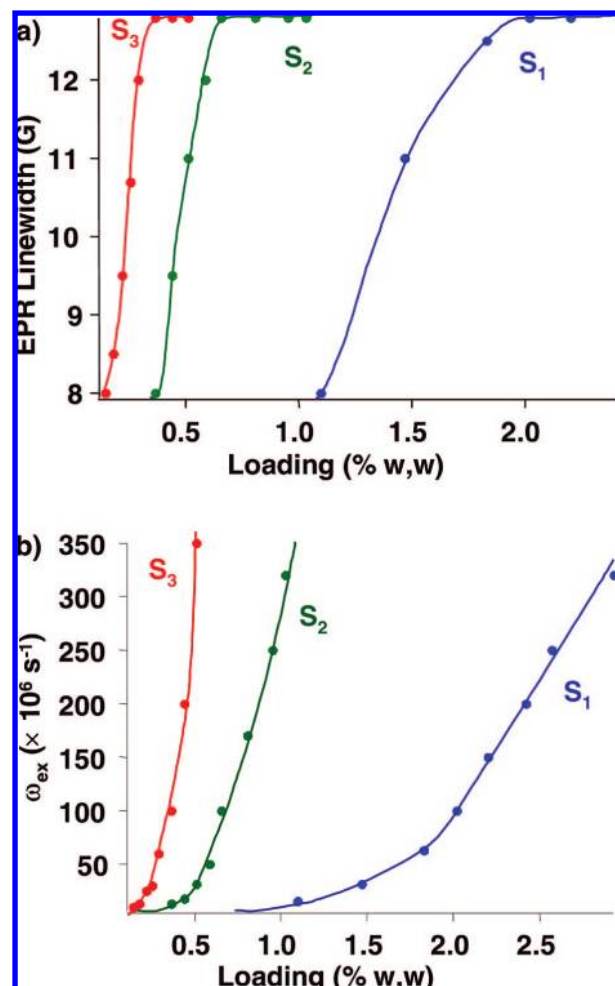
Figure 9. Behavior of (a) the EPR line width and (b) the spin−spin exchange frequency versus 4-DPA-TEMPO surface loading. These parameters are EPR spectra simulation outputs. When the line width reaches the plateau, the strong binding sites are saturated. Solid lines are for clarity only and do not have physical meaning.

distance between the probes remains essentially the same (the dipolar broadening reaches a plateau, as shown in Figure 9a for silicates S_1, S_2, and S_3.) the local concentration of radical adsorbed increases constantly with loading, as demonstrated by the larger and larger values of ω_{ex}. This is explained in the light of the two-binding-sites paradigm, assuming that the strong binding sites are saturated at c^* and that above c^* the probe mobility and diffusion increase dramatically, producing a high collision frequency between probe molecules. These dynamic features are reflected in the EPR spectrum as increasing spin−spin exchange frequency (Figure 9b).

A more rigorous test of the model is provided by the investigation of a systematic series of monodisperse crystals of differing size, since the number of available pore openings (strong binding sites) is related to the crystal size. From knowledge of the crystal size, the critical loading and the external surface should have a direct relationship, namely $S_{tot} = lS_{ext}$ (eq 2). Thus, a plot of S_{tot} versus S_{ext} is expected to yield a straight line, within the limits of the approximation of eq 2. Since S_{tot} is proportional to the EPR-determined critical loading c^* and S_{ext} is proportional to the external surface area, a linear relationship between c^* and the external surface area is expected. Since the external surface area, in turn, is related
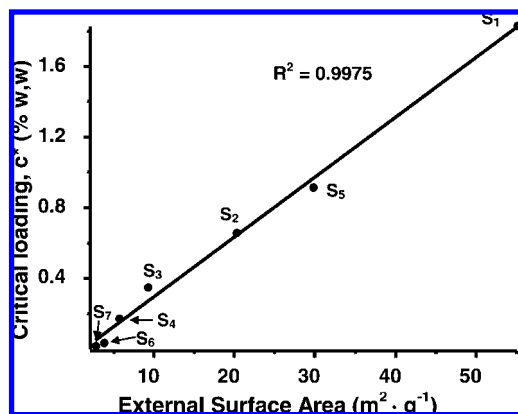
Figure 10. Critical loading of nitroxide 4-DPA-TEMPO versus external surface area for different monodisperse silicalites. The two parameters show a strong linear relationship, providing significance to the EPR analysis for the titration of the strong binding sites of the external surface of MFI crystals.

Figure 11. FT-IR spectum of *o*-MeDBK@MFI at different loadings. The two peaks correspond to the two sites of interaction with the external surface of zeolite: 1716 cm^{-1} (weak binding sites) and 1696 cm^{-1} (strong binding sites). (Inset) FT-IR spectrum of 5% loading *p*-MeDBK@MFI (black line) and 5% loading *o,o'*-diMeDBK@MFI (blue line). The three peaks for *p*-MeDBK record the three sites of interaction with the zeolite: 1716 and 1696 cm^{-1} are for the external surface, whereas 1685 cm^{-1} is for the internal pores (blue); for *o,o'*-diMeDBK there is only one peak in this case for the interaction of the adsorbate molecule with the weak binding sites on the external surface, as it cannot intercalate inside the pore openings. These spectra refer to silicalite S$_7$.

to the crystal size, *a linear relationship is expected between c* and the crystal size.*

This rather rigorous test of the model requires determination of the external surface area of a set of monodisperse crystals of varying size. Accordingly, a set of monodisperse silicalite crystals of external surface area varying from ∼3 to ∼50 m^2 g^{-1} were synthesized (Table 2).The external surface area was measured by mercury porosimetry, a widely used technique to determine the external surface area of porous materials,[46,47] while c* was obtained by the EPR analysis described above for 4-DPA-TEMPO as a probe. Figure 10 reports the plot of c* versus external surface area for seven silicalites with different particle sizes: the linear relationship strongly validates the critical loading, c*, as a quantitative parameter for characterization of the external surface of silicalites crystals. Furthermore, from simulation of the spectra, the probe distance corresponding to c* remains constant throughout all the zeolite samples at ∼13 Å (Table 2). The c* values for 4-DPA-TEMPO were also calculated from the external surface areas by assuming two holes per 330 Å^2 (average of the two different faces of the MFI crystals). The calculated versus measured values of c* show good agreement, within the experimental error (Table 2).

In order to adapt this approach to more commonly available materials, we tested a second probe, 4-oxo-TEMPO, and the laboratory-synthesized silicalite S$_7$ and compared the results to those obtained with a commercial zeolite. The EPR analysis shows very good agreement for 4-oxo-TEMPO with the results for 4-DPA-TEMPO probe (Table 2), within the error limit of the computer-aided spectral simulation. Next, 4-oxo-TEMPO was adsorbed on commercial MFI zeolites with different Al contents. The critical loading, which ranges between 0.013 and 0.051%, is reported in Table 2, along with the correspondent average probe distances. Although these zeolites have the same nominal particle size of 2 μm, their high polydispersity does not permit a linear relationship between c* and the external surface area. However, the average probe distance at c*, which depends only on the crystal structure, remains constant for all the commercial zeolites tested and is in very good agreement with the XRD data for pore opening distance. This demonstrates the utility of EPR analysis for the determination of critical
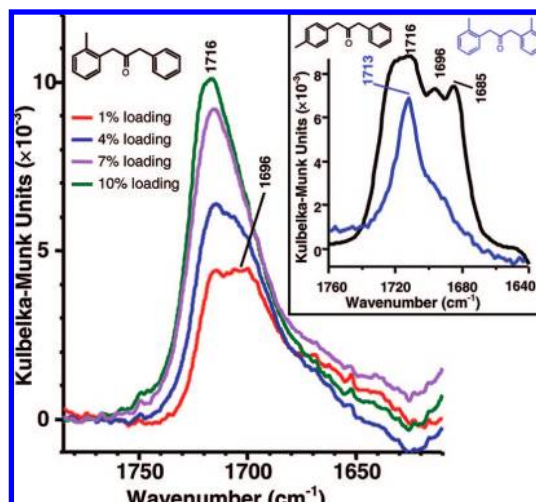
loading, hence the method for the "titration" of the surface pore openings, e.g., the strong binding sites, independent of Al content.

FT-IR Analysis: Three Peaks for Three Types of Interactions. Infrared spectroscopy is a powerful tool for the investigation of the interactions between adsorbed molecules and surfaces, because binding sites of different strengths cause a shift in a probe's vibrational peaks in the FT-IR spectrum. For example, in a nonpolar solution phase, the carbonyl stretch, $\nu(CO)$, of *o*-MeDBK and *p*-MeDBK occurs at the same frequency, ∼1717 cm^{-1}. In polar media, $\nu(CO)$ shifts to lower energies. Thus, it is expected that a ketone probe adsorbed on a MFI zeolite will exhibit values of $\nu(CO)$ that are related to the polarity of its binding site. Since the more polar binding sites are expected to be more strongly binding, the shift to lower energy should be a signature of interactions with the strong binding sites. It is natural, therefore, to consider how FT-IR spectroscopy can be employed to provide information on the binding of the ketones studied in this investigation (Chart 1).

In Figure 11, the FT-IR spectrum of *o*-MeDBK@MFI is shown at different loadings. At 1% loading, two peaks at 1716 and 1696 cm^{-1} are present; this provides direct evidence to support the two-site binding model of the external surface of zeolites. The weak binding site interaction is assigned to the peak at 1716 cm^{-1}, because this value most closely matches that of *o*-MeDBK in solution, whereas the interaction with the strong binding sites produces the peak at 1696 cm^{-1}. This is even more convincing if compared with the inset of Figure 11, where the FT-IR spectrum of *p*-MeDBK@MFI is reported for an intermediate loading. In accordance with the assumption that *p*-MeDBK can diffuse inside the zeolites pores, three different $\nu(CO)$ energies are centered at 1716, 1696, and 1685 cm^{-1}. The first two, being also present in the spectrum of *o*-MeDBK, are assigned to the interaction with the external surface, whereas the third one, at the lowest frequency, corresponds to the interaction with the internal pores of the MFI zeolite.

(46) Gregg, S. J.; Sing, K. S. W. *Adsorption, surface area, and porosity*; Academic Press: London, 1982.
(47) Abrams, L.; Keane, M.; Sonnichsen, G. C. *J. Catal.* **1989**, *115*, 410.
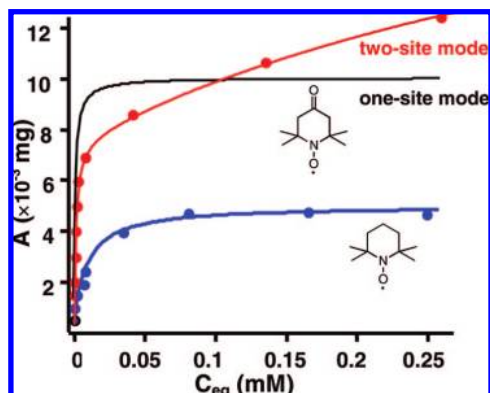
Figure 12. Langmuir isotherm for 4-oxo-TEMPO and TEMPO adsorbed onto silicalite S_7. While the experimental points of 4-oxo-TEMPO can only be fitted by a two-site model (eq 4), TEMPO is well fitted by a one-site model, i.e., $K_w = 0$. A summary of fitting parameters is reported in Table 3.

Table 3. Langmuir Isotherm Fitting Parameters

molecule	M_s (mg)	k_s	M_w (mg)	k_w
o-MeDBK[a,b]	0.40	350	0.59	2.1
o,o'-diMeDBK[b]	0	0	1.0	10
4-oxo-TEMPO[c]	0.37	1090	0.63	2.0
TEMPO[c]	1.0	115	0	0

[a] Reference 20. [b] For MFI with Si/Al = 20. [c] For silicalite S_7.

In order to fully test the external surface model, we completed the cases sketched in Figure 2 measuring the FT-IR spectrum of o,o'-diMeDBK@MFI, a molecule that is unable to intercalate a benzene ring inside the channels, and thus unable to occupy the strong binding sites. The spectrum (lower trace in the inset of Figure 11) shows predominantly only one peak centered at 1713 cm^{-1}, confirming the prediction of the model.

Langmuir Isotherm. The model and the spectroscopic experimental evidence presented above clearly demonstrate that there is both a strong binding site and a weak binding site associated with the external surface of MFI zeolite. Additional evidence for the presence of two binding sites with different energies on a surface is obtained by constructing the classical Langmuir isotherm for the probes investigated in this study. Moreover, a fit of the isotherm allows a quantitative estimation of the binding energies of the strong and weak binding sites.[48] The Langmuir isotherm for o-MeDBK@MFI (Si/Al = 20) is reported in the literature and shows the two binding sites' behavior.[16] We constructed the Langmuir isotherm for 4-oxo-TEMPO, in order to ensure that our EPR analysis was indeed consistent with the two-site model. The result is shown in Figure 12. The best one-site fitting curve is clearly not appropriate in this case; however, the two-site curve offers a good agreement with the experimental data. The analytical expression of the Langmuir fitting curve is given by eq 4, while the best fitting parameters for 4-oxo-TEMPO and o-MeDBK are summarized in Table 3.

$$A = M_s \frac{k_s C}{(1 + k_s C)} + M_w \frac{k_w C}{(1 + k_w C)} \quad (4)$$

In eq 4, A (in mg) is proportional to the surface coverage, C is the total loading of the adsorbate (in wt/wt), M_s and M_w give an estimation for the relative coverage of strong and weak sites,

respectively, by the adsorbate (in mg), and k_s and k_w are related to the equilibrium constants for the adsorption onto the strong and weak sites, respectively.

The parameters in Table 3 show that 4-oxo-TEMPO binds about 3 times more strongly with the strong binding sites than o-MeDBK. This can be due to (i) a reduced steric hindrance because of the absence of bulky phenyl groups, (ii) a different approach of the molecule to the binding sites that modifies the thermodynamics of the interaction, or (iii) the fact that 4-oxo-TEMPO binds with the zeolite surface also through the N—O• moiety. For comparison, the Langmuir isotherm for TEMPO was also constructed. In this case, no carbonyl group is present, and the experimental data can be fit with the one-site model (Figure 12). The fitting parameters reported in Table 3 show a value of k_s about 100 times lower for TEMPO than for 4-oxo-TEMPO, confirming the assumption that the carbonyl group is largely responsible for the adsorption of the latter molecule, as the N—O• group itself interacts very poorly with the zeolite surface. With such a low interaction energy, the weak binding sites are not effective in binding TEMPO ($k_w = 0$); this results in a one-site model fitting of the Langmuir isotherm. Moreover, comparing the value of M_s for 4-oxo-TEMPO (converted to coverage percentage), which gives an estimation of the maximum amount of adsorbate needed to occupy all the strong binding sites, with the value of c^* for the same probe in silicalite S_7, we found them in reasonable agreement, $M_s = 0.0155\%$ and $c^* = 0.0180\%$, to confirm the accuracy of our EPR approach.

Finally, the Langmuir isotherm for the o,o'-diMeDBK is constructed. Since such ketones cannot intercalate into the pore openings of the zeolite crystals as o-MeDBK can, a weaker interaction with the external surface of zeolite is expected, as observed in its FT-IR spectra, which shows one slightly shifted peak. The experimental data can again be fitted with the one-site adsorption model (Table 3). The value $k_w = 10$ implies an interaction with the surface more than an order of magnitude weaker than for o-MeDBK on the same type of crystals (Si/Al = 20). In light of consistent FT-IR measurements, it is concluded that, for dibenzyl ketones, the strong binding sites on the external site of the zeolite are due to the intercalation of part of the molecule into the pore openings; if this is impeded, as in the case of o,o'-diMeDBK, interaction energies are significantly lower, by up to an order of magnitude, typical of interaction with weak binding sites. This simple comparison validates the postulate that the strong binding sites are the pore openings of the external surface of the zeolites.

Conclusions

The impact of the external surface on the physical−chemical properties of zeolites increases with decreasing particle size. In order to optimize zeolites' performances, knowledge of the external surface adsorption properties is essential. A model in which the external surface of zeolites is composed of strong binding sites, located on the pore openings, and weak binding sites, situated between the pores, has been extensively investigated using a multi-technique approach.

FT-IR spectroscopy has been used to show directly the three types of interactions, characterized by different ν(CO) peak shifts, that selected dibenzyl ketones (Chart 1) can have with the zeolite framework. The weak and strong sites on the external surface are clearly revealed by ν(CO) at 1716 and 1696 cm^{-1}, respectively (Figure 11).

(48) Ościk, J. *Adsorption*; Halsted Press: New York, 1982.

By EPR spectroscopy, a direct method to specifically probe the strong binding sites on the external surface of MFI zeolites has been developed. A measure of the critical loading, c^*, at which the strong binding sites are saturated and cross-comparison with mercury porosimetry and XRD data validates the EPR method for characterizing the external surface of MFI zeolites. The exact value of the external surface area for monodisperse silicalites can be determined by the EPR spin probing method described here, provided that a pre-characterized and calibrated silicalite sample is available as a standard.

The interaction energies for the dibenzyl ketones and the nitroxides used as EPR probes have been determined by measuring the Langmuir isotherm. The results are consistent with a two-site energy surface in which the intercalation of the unsubstituted benzene ring of *o*-MeDBK inside the channels system provides the most significant contribution to the interaction energy for the adsorption to the external surface of zeolite. Other mechanisms, such as hydrogen-bonding and van der Waals interactions, are more than an order of magnitude less intense, as demonstrated by the *o,o'*-diMeDBK Langmuir adsorption isotherm (Table 3); these interactions are typical of the weak binding sites. Since the latter molecule cannot intercalate inside the pore openings because of structural impedances, previous assignment of the strong binding sites to the pore openings proves to be correct in the light of the present investigation.

Finally, the photochemistry of *o*-MeDBK@MFI and DBK@MFI (Scheme 1) in the presence of spectator molecules, such as water, pyridine, and benzene, has been investigated both by measuring the concentration of final products to calculate the cage effect and by following the persistent benzyl and acyl radicals in real time by cw-EPR spectroscopy. The presence of co-adsorbed spectator molecules adds another level of variability to this supramolecular system for adjusting and controlling the product distribution of such radical reactions. In particular, it has been found that, during the photolysis of DBK@MFI in the presence of pyridine and benzene, the decarbonylation step is slowed so greatly that the phenylacetyl radical becomes persistent (time scale of minutes) and thus detectable by cw-EPR: a remarkable outcome, if compared to the sub-microsecond time scale for the decarbonylation step for dibenzyl ketones in solution.[49,50]

Experimental Section

Materials. Syntheses of 1,3-diphenyl-2-propanone (DBK), 1-(2-methylphenyl)-3-(phenyl)-2-propanone (*o*-MeDBK), their deuterated benzene counterparts, and 1,3-bis(2-methylphenyl)-2-propanone (*o,o'*-diMeDBK) were performed as previously reported,[29] as was that of 1-(4-methylphenyl)-3-phenyl-2-propanone (*p*-MeDBK).[51] Pyridine, benzene, and *p*-xylene were purchased from Aldrich and used as received.

Nitroxide probe 2,2,6,6-tetramethyl-4-[(diphenylacetyl)oxy]-1-piperidinyl-oxy (4-DPA-TEMPO) was synthesized following a published procedure for esterification at room temperature, using 4-hydroxy-2,2,6,6-tetramethyl-1-piperidinyl-oxy and diphenylacetic acid, in 66% yield.[52] It was recrystalized using ethyl acetate. MS (FAB$^+$): 366.2 (M − H)$^+$, 368.2 (M + H)$^+$. Nitroxide probes
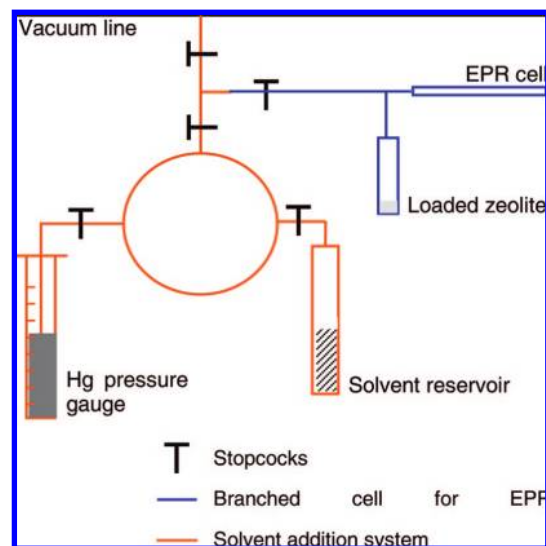

Figure 13. Schematic representation of the home-made apparatus used for loading zeolites with spectator solvent molecules. It is composed of two parts: a branched cell for EPR measurements (blue line), where the zeolite, previously loaded with DBKs, is placed and that will also serve as EPR sample holder, and the solvent addition system (orange line), where a controlled vapor pressure can be created and then let adsorb to the loaded zeolite. All parts are made of Pyrex glass, except for the EPR cell, which is made of quartz for irradiation.

4-oxo-2,2,6,6-tetramethyl-1-piperidinyl-oxy (4-oxo-TEMPO) and 2,2,6,6-tetramethyl-1-piperidinyl-oxy (TEMPO) were purchased from Aldrich and used without further purification.

Laboratory-synthesized, monodisperse silicalite crystals (S_n) were synthesized and fully characterized as described in a previous publication.[18] Commercial zeolited (C_n) were purchased from Zeocat. It is important to emphasize that initial studies using amorphous silicalites (defect laden) showed the same photochemically induced reaction outcome as did those using the highly crystalline zeolite.[27,47] Therefore, within measurement and calculation error, perfect, monodispense crystals have been assumed.

EPR Analysis with Nitroxide Spin Probes. In a typical experiment, 300 mg of calcined zeolites was first activated in an aerated furnace at 500 °C for 2 h and then placed in a desiccator to allow cooling to room temperature before use. Next, 3 mL of solution in 2,2,4-trimethylpentane (isooctane), containing an appropriate amount of adsorbate molecule, was added to the activated crystal. Isooctane was chosen as solvent because of its inability to penetrate the pore openings of the MFI zeolite, as its kinetic diameter is larger than the pore openings.[53] The system was allowed to equilibrate under magnetic stirring for about 10 h. To obtain the dry loaded sample, the solvent was first removed under gentle Ar stream, and then the sample was degassed under vacuum (1×10^{-5} Torr) in a branched EPR cell (Figure 13, blue line). Measurements were performed using an EMX Bruker spectrometer with a microwave power of 2.01 mW and modulation amplitude of 1.0 G. Spectral simulations were made using the software NLSL for slow tumbling motion regime.[54,55] The simulation strategy approach is described in detail elsewhere.[19]

FT-IR Measurements. Preparation of loaded zeolite followed closely that for EPR measurements except for the amount of zeolite used, which in this case was typically 20 mg, and the total volume

(49) Gould, I. R.; Baretz, B. H.; Turro, N. J. *J. Phys. Chem.* **1987**, *91*, 925.

(50) Tsentalovich, Y. P.; Kurnysheva, O. A.; Gritsan, N. P. *Russ. Chem. Bull.* **2001**, *50*, 237.

(51) Hrovat, D. A.; Liu, J. H.; Turro, N. J.; Weiss, R. G. *J. Am. Chem. Soc.* **1984**, *106*, 5291.

(52) Hassner, A.; Alexanian, V. *Tetrahedron Lett.* **1978**, 4475.

(53) Jacobs, P. A.; Martens, J. A.; Weitkamp, J.; Beyer, H. K. *Faraday Discuss.* **1981**, *72*, 353.

(54) Budil, D. E.; Lee, S.; Saxena, S.; Freed, J. H. *J. Magn. Reson., Ser. A* **1996**, *120*, 155.

(55) Earle, K. A.; Budil, D. E. In *Advanced ESR Methods in Polymer Research*; Schlick, S., Ed.; Wiley-Interscience: Hoboken, NJ, 2006.

(56) Hill, S. G.; Seddon, D. *Zeolites* **1985**, *5*, 173.

of adsorbate solution, which was 200 μL. After drying in the vacuum line, 5 mg of loaded zeolite was combined with 500 mg of commercially prepared KBr crystals (purchased from Thermo). The diffuse reflectance infrared spectroscopy by Fourier transform (DRIFT) technique was used for these measurements. The FT-IR spectra were obtained at room temperature on a Nicolet Nexus 360 spectrometer (equipped with a DTGS detector and DRIFTS Smart accessory) at 2 cm^{-1} resolution, 64 scans.

Photolysis of DBKs and Cage Effect Measurement. Dibenzyl ketones and spectator molecules were loaded to the zeolite in two separate stages. First, the desired DBK was loaded following the procedure described for the EPR analysis; however, CH$_2$Cl$_2$ was used in this case as solvent to allow the solution to permeate inside the pores of the zeolite. The zeolite was placed in a branched cell for EPR measurements (Figure 13, blue line) and dried under vacuum at 1×10^{-5} Torr. At this point, spectator molecules were added by a solvent addition system (Figure 13, orange line). This system, designed in-house by X.L. and manufactured by Mr. Fred Krummer (glassblower), is composed of a 250 mL round-bottom flask connect to a mercury pressure gauge, which was calibrated before use, a solvent reservoir containing 1 mL of liquid, which was degassed by pump−freeze−thaw cycles before addition to the zeolite, the branched cell for EPR measurements, and a vacuum line. To add a desired amount of solvent to the zeolite, we first evacuated the whole system (except the solvent reservoir) to 1×10^{-5} Torr and then, closing the connections to the vacuum line and to the branched cell, let the solvent vapors occupy the rest of the volume. The vapor pressure in these conditions was calculated by the movement of the mercury column. The amount of solvent to be added to the zeolite was converted to the pressure difference and mercury level, according to the volume of the total system and the molecular weight of the solvent. The last step was to open the connection to the EPR branched cell until the desired mercury level was reached. The system proved to be very accurate, as the solvent loading error caused by the mercury level reading is less than 2%.

It is important to highlight that the dibenzyl ketone is loaded before the spectator molecule for the following reasons: (i) to be consistent with similar studies previously reported in which water was used as spectator molecule[27] and (ii) to make sure that the photolysis of DBKs is studied starting from the same conditions of zeolite loading, allowing a more straightforward comparison among the spectator molecules.

For the cage effect measurement, the loaded, degassed zeolite was irradiated with a 450 W medium-pressure Hg lamp through a chromate filter solution with continuous cell tumbling. The conversion of the reaction was controlled to less than 25%, and the irradiated samples were extracted with ether or benzene. The product distribution was measured by GC. For the kinetics measurements with cw-EPR, the branched cell was put inside the EPR cavity and irradiated for 6 s with a 300 W Xe lamp with an optical filter to cut the wavelengths below 300 nm. The EPR spectra or the time decays were recorded immediately after the photolysis.

Langmuir Isotherms. Langmuir isotherms were constructed using a standard depletion method, in which the amount of adsorbed molecule was calculated from the difference between the initial and the final concentrations in the solution. This was followed by doubly integrated EPR spectra for nitroxides and absorption at 295 nm for *o,o′*-diMeDBK. Starting solutions were prepared in isooctane and added to 200 mg of zeolite. The system was allowed to equilibrate under magnetic stirring for about 10 h before measuring the concentrations of the supernatant.